THE ASTROPHYSICAL JOURNAL, 456:132–140, 1996 January 1

A 21 CENTIMETER ABSORBER IDENTIFIED WITH A SPIRAL GALAXY: *HUBBLE SPACE TELESCOPE*[1] FAINT OBJECT SPECTROGRAPH AND WIDE-FIELD CAMERA OBSERVATIONS OF 3CR 196

ROSS D. COHEN, E. A. BEAVER, ATHANASSIOS DIPLAS, VESA T. JUNKKARINEN,
THOMAS A. BARLOW, AND RONALD W. LYONS
Center for Astrophysics and Space Sciences 0111, University of California, San Diego, 9500 Gilman Drive, La Jolla, CA 92093-0111
Received 1994 December 7; accepted 1995 July 5

ABSTRACT

We present imaging and spectroscopy of the quasar 3CR 196 ($z_e = 0.871$), which has 21 cm and optical absorption at $z_a = 0.437$.

We observed the region of Lyα absorption in 3CR 196 at $z_a = 0.437$ with the Faint Object Spectrograph on the *Hubble Space Telescope*. This region of the spectrum is complicated because of the presence of a Lyman limit and strong lines from a $z_a \approx z_e$ system. We conclude that there is Lyα absorption with an H I column density greater than 2.7×10^{19} cm^{-2} and most probably 1.5×10^{20} cm^{-2}. Based on the existence of the high H I column density along both the optical and radio lines of sight, separated by more than 15 kpc, we conclude that the Lyα absorption must arise in a system comparable in size to the gaseous disks of spiral galaxies.

A barred spiral galaxy, previously reported as a diffuse object in the recent work of Boissé & Boulade, can be seen near the quasar in an image taken at 0".1 resolution with the Wide Field Planetary Camera 2 on the *HST*. If this galaxy is at the absorption redshift, the luminosity is approximately L_*, and any H I disk should extend in front of the optical quasar and radio lobes of 3CR 196, giving rise to both the Lyα and 21 cm absorption.

In the $z_a \approx z_e$ system we detect Lyman lines and the Lyman limit, as well as high ion absorption lines of C III, N V, S VI, and O VI. This absorption probably only partially covers the emission-line region. The ionization parameter is approximately 0.1. Conditions in this region may be similar to those in broad absorption line QSOs.

Subject headings: galaxies: ISM — quasars: absorption lines — quasars: individual (3CR 196) — radio lines: galaxies

1. INTRODUCTION

The total H I mass indicated by the damped Lyα absorption systems in QSO spectra at high redshift is similar to the baryonic mass in spiral galaxies at the present epoch (Lanzetta et al. 1991) and thus constitutes a major component of the baryonic matter in the universe. Evidence that the damped Lyα systems are the progenitors of spiral galaxies includes: the large column density of H I, the presence of metals, and the presence in the gas of both a turbulent and quiescent component, which is dominated by low-ionization absorption (Wolfe et al. 1986; Turnshek et al. 1989; Lanzetta et al. 1991). The systems at $z \gtrsim 2$ differ from present-day spirals in the inferred sizes or number density of the disks (see references above) as well as in the metal abundances (Pettini et al. 1994), dust contents (Fall, Pei, & McMahon 1989; Pei, Fall, & Bechtold 1991; Lanzetta, Wolfe, & Turnshek 1989), molecular fractions (Black, Chaffee, & Foltz 1987; Foltz, Chaffee, & Black 1988; Chaffee, Black, & Foltz 1988; Lanzetta, Wolfe, & Turnshek 1989), and spin temperatures (see Briggs 1987 for a review; Cohen et al. 1994). These features might be expected of disk progenitors.

There is no proof, however, that the damped Lyα systems cannot also arise in halo components or dwarf galaxies (York et al. 1986). In fact, Meyer & York (1992) argue that the low metal abundances seen in the damped Lyα absorption system in the spectrum of 3CR 286 ($z_a = 0.692$; see also Cohen et al. 1994) imply that the damped Lyα systems come from a slowly evolving population and do not represent disk progenitors.

Among the goals of studies of damped Lyα systems are the determination of the morphology of the absorbers and direct measurements of the sizes of the gaseous components. Observations of PKS 0458−020 offer the most convincing evidence for a large, disk-like absorber. The damped Lyα system ($z_a = 2.04$) seen in the optical point source (Wolfe et al. 1985) is also seen in 21 cm absorption against the extended radio source and covers at least 24 h^{-1} kpc (Briggs et al. 1989).[2] Observations of low-redshift damped Lyα systems, where the morphology of the absorber can be determined from *Hubble Space Telescope* (*HST*) images, may allow us to determine the population of objects included among the high-redshift systems. The absorbers have probably been identified in ground-based images for three low-redshift damped Lyα systems, but their morphology has not been determined (Steidel et al. 1994b, 1995). Until the advent of the *HST*, low-redshift systems had been found primarily with 21 cm absorption. If the Lyα region is observed along the radio line of sight, an object with 21 cm absorption should show a damped Lyα system, allowing a

[1] Based on observations with the NASA/ESA *Hubble Space Telescope*, obtained at Space Telescope Science Institute, which is operated by AURA, Inc., under NASA Contract NAS 5-26555.

[2] We use $h = H_0/50$ km s^{-1} Mpc^{-1} and $q_0 = 0.05$ throughout.

determination of the spin temperature (T_s). If the lines of sight differ, we can limit the size of the gaseous component of the absorber. In either case, if we measure Lyα, we can combine the H I measurements with high-resolution measurements of metal lines to measure absolute abundances as functions of galaxy type, impact parameter, and redshift.

3CR 196 (0809+483, $V = 17.7$, $z_e = 0.871$), a radio source with a weak core and lobes separated by approximately 5″, shows 21 cm absorption in two components (Brown & Mitchell 1983) at $z_a = 0.436576$, 0.436669. These components are separated by 19 km s^{-1}, and each has Doppler parameter $b \approx 10$ km s^{-1}. The absorption line depth is much greater than the flux in the central point source, and a VLBI nondetection (Brown et al. 1988) limits the absorption against the most compact hot spot, requiring that a significant fraction of the absorption be formed in an extended region. The diameter of the absorber thus exceeds 0.″63, or 4.7 h^{-1} kpc,[3] and the column density exceeds $8.6 \times 10^{17} T_s$. Optical absorption in Mg II, Fe II, and Mn II (discovered by Foltz, Chaffee, & Wolfe 1988, hereafter FCW) has b of 75–130 km s^{-1} at $z_a = 0.43685$, which differs from the 21 cm redshift by only 50 km s^{-1}. The combination of optical and radio absorption sets a lower limit to the size of the overall structure of approximately 15–20 h^{-1} kpc, but the high velocity dispersion implies the gas is halo-like, not disk-like, and therefore the size does not necessarily refer to the size of any H I disk. FCW also detect a Mg II absorption system at $z_a = 0.8714$, close to the emission-line redshift.

A wisp of emission (Matthews & Sandage 1963) was shown to be an object of galaxy-like dimensions centered approximately 1.″7 southeast of the quasar (Boissé & Boulade 1990, hereafter BB). If this is the origin of the $z_a = 0.437$ absorption, then H I might extend in front of the optical quasar, giving rise to a damped Lyα line.

We report here on *HST* observations[4] including both Wide Field Camera (WFC) images of the 3CR 196 field and low-resolution Faint Object Spectrograph (FOS) observations of the $z_a = 0.437$ Lyα absorption feature, as well as UV lines in the $z_a = 0.871$ associated system. These observations were intended to determine the type of galaxy responsible for the 21 cm absorption and the extent of the H I gas. The observations, reductions, and measurement techniques are described in § 2. The results are described in § 3 (§ 3.4 gives some results on the $z_a = 0.871$ system). Some implications are discussed in § 4.

2. OBSERVATIONS, REDUCTIONS, AND MEASUREMENTS

2.1. *Images*

Two 10 minute exposures of 3CR 196 were obtained with the optically corrected WFC on *HST* on 1994 March 24. They were obtained with the F702W filter and have a scale of 0.″0966 pixel^{-1} (Trauger et al. 1994). The averaged image is shown in Figure 1 (Plate 1). We have superposed the 6 cm radio contours (generously provided by A. Oren) by assuming that the position of the central radio source is coincident with the optical quasar. The QSO image is saturated in the core and has strong diffraction spikes, one of which crosses a spiral galaxy southeast of the QSO. This is the object identified as the probable absorber by BB. The spiral galaxy also sits on the wings of the approximately r^{-3} QSO scattered light function (Bartko et al. 1993). North of the QSO is a fainter object (also seen by BB) which is resolved but does not clearly show galactic features.

Data reduction was performed with the pipeline reduction system and the most recent calibrations available at the time of reduction; these were generally ground-based calibrations. The images were averaged using the STSDAS task "combine" with the "crreject" keyword to reject points that are unexpectedly high in one of the two images, presumably because of cosmic rays. The number of hot pixels increases with time after a WFC decontamination procedure; they are not removed by the cosmic-ray rejection routine because they occur in both images. Single hot pixels in the region of interest were identified and removed from the averaged image by spatial median filtering; this effectively removes hot pixels in regions where the image has little structure. Dark exposures taken 1 day before and 1 week after the 3CR 196 images do not show any hot pixels in regions where the median filtering technique would not work well.

2.1.1. *QSO Point Source Subtraction*

The diffraction spikes and scattered light function must be subtracted prior to any measurements of the galaxy. We used the "Tiny Tim" optical simulation code (v. 4.0) (Krist 1993) to create a point-spread function (PSF) sampled very 0.1 pixel at the approximate position of the QSO. We added together monochromatic PSFs at 10 wavelengths equally spaced across the F702W filter passband, weighted by the total instrument throughput and photon flux of the object.[5]

To include subpixel variations and scattered light within the CCD, the PSF was convolved with the CCD pixel spatial response (J. Krist, private communication). The PSF was resampled at the original pixel scale and iteratively subtracted from the image by varying the PSF centroid position and peak intensity, minimizing χ^2 in an annulus that excluded both the saturated core and the region of the wings where the galaxy and other features are prominent. The best fit yields a total of 63,100 counts in the PSF, which has 13,100 counts in the peak pixel, much higher than the maximum counts in the southeast galaxy, 38 counts above background. The subtracted image is shown in Figure 2 (Plate 2). The degree of success of the subtraction can be seen in the incomplete subtraction of the diffraction spikes in the regions of the image unaffected by galaxy images. Although the spikes are largely removed, positive and negative residuals remain, indicating that a perfect subtraction is not possible with our PSF. However, the errors are small compared to the counts in the galaxy.

2.1.2. *Magnitude Scale*

The *HST* magnitude system is based on f_λ (Koornneef et al. 1988) and can be converted to m_v at the "pivot wavelength" of 6942.46 Å. This approximates the monochromatic AB 79 system (Oke & Gunn 1983). To translate to an approximate broadband R magnitude, which is centered at approximately 7000 Å, we subtract 0.25 mag, the relative magnitude of Vega at 7000 Å with respect to 5556 Å (Hayes & Latham 1975). To compute broadband rest frame B magnitudes, we apply a K-correction consisting of a bandpass term of $1 + z$ and an

[3] At the redshifts of interest for 3CR 196, $z = 0.437$ and $z = 0.871$, 1.″0 corresponds to 7.4 h^{-1} kpc and 10.1 h^{-1} kpc, respectively.

[4] Observations with FOS and WFC were obtained as part of GHRS GTO programs 1193, 3939, and 5176.

[5] The photon flux was determined from large-aperture, low-resolution optical spectra obtained at Lick Observatory on 1993 February 1 with the 3 m Shane Telescope and CCD spectrograph under photometric conditions.

approximate correction based on the ratio of a galaxy flux at 6942.46 Å/(1 + z) to the galaxy flux at 4400 Å in the rest frame (based on spectra of Sc galaxies in Kennicutt 1992). This latter correction is a factor of 1.07 for $z = 0.437$ and 1.38 for $z = 0.871$. We then add 0.24 mag to translate to a broadband B magnitude.

2.2. *Spectra*

Two spectra of 3CR 196 covering the region from 1600 Å to 2415 Å were obtained with the pre-COSTAR FOS on the *HST* using the low-resolution UV grating (G160L) and the red detector. The first observation, intended as a flux measurement to determine the exposure time for an observation at higher resolution, was done in ACCUM mode on 1991 December 4. The exposure through the target acquisition aperture (full width at half-maximum [FWHM] $\approx$ 10 Å) totaled 1200 s. We determined that a useful high-resolution spectrum with the smaller apertures could not be obtained in a reasonable time, given the light loss due to the aberrated *HST* PSF, but a longer spectrum with the G160L and 1".0 aperture (FWHM nominally 8.6 Å and lacking the strong wings present with the 4".3 aperture) would be satisfactory. This second observation was made on 1992 September 26 with the FOS in the RAPID mode and totaled 8689 s. FOS spectra are quarter stepped to improve the sampling, so the exposure time per quarter-diode pixel is one-quarter of the total exposure time.

The spectrum from the second exposure is shown in Figure 3*a*, with the strongest absorption features identified. They include H I and high ions in the $z_a \approx z_e$ system: N V, Lyα, blends of Lyβ/O VI and Lyγ/C III, and Lyδ. It is immediately apparent that the Lyα/Lyβ ratio is anomalous. At $z_a = 0.437$, lines of C IV and Si II λ1526 and a strong feature near the expected position of Lyα are the only lines that can be reliably identified.

2.2.1. *Reduction Procedures*

The second observation was reduced with the FOS GTO team's IDL CALFOS routines and was processed as it would have been with the standard reduction software, with the exceptions noted below.

In order to minimize the impact of the cyclic drift of the spectrum on the diode array (GIM), the spectrum was read out approximately every 37.2 s using RAPID mode, and the data were shifted before coadding, following a model of Earth's magnetic field (Junkkarinen et al. 1992) and a model of the shift that incorporates two different coefficients for observations with and without prior de-Gaussing (Lyons et al. 1994).

Important uncorrected sources of error in the wavelength zero point include uncertainty in centering the object in the aperture (typically $\pm$1.5–3 Å with this configuration [Caganoff, Tsvetanov, & Armus 1992]) and errors in the setting of the filter/grating wheel (FGW). The peak-to-peak range of this variation is 4.1 quarter-diode pixels, or 7.1 Å ($1\sigma = \pm 1.4$ Å) (Lyons et al. 1994), and the error in the wavelength zero point of our spectrum could be positive or negative by up to this amount depending on the setting of the FGW during the wavelength calibration exposure itself. The measured wavelength of Si II λ1526 in the $z_a = 0.437$ absorption system (see § 2.2.2) differs from the predicted wavelength in the similarly reduced wavelength calibration by approximately -10 Å. Since this line is strong and likely to be unblended, the final wavelength calibration was adjusted by this amount. This adjustment puts the blended C IV doublet at this redshift at approximately the correct wavelength and also brings the redshifts of the H I lines in the $z_a = 0.871$ system into better agreement with each other and with the redshift determined from the optical lines. The wavelength shift is barely consistent with the expected range of variation but is similar to that seen in 3CR 286 (Cohen et al. 1994).

Both the sensitivity and the diode-to-diode response of the red detector are slowly changing in the 1900–2050 Å region—the region of the Lyβ/O VI absorption—but the short interval (<2 months) between the data and flat-field calibration (1992 November 21) minimizes errors due to flat-field variations. Comparison of two flat-field exposures taken 1 month apart shows variation of 2% peak to peak (smaller than the photon counting noise in the 3CR 196 spectrum) on a 1–2 diode scale, and 5% peak-to-peak variations on a scale of 150 Å. The inverse sensitivity calibration of 1992 March was used. Variations in the sensitivity calibration on this timescale could be significant, but they occur over a longer wavelength range than the features being measured here.

Despite standard background subtraction (Lyons et al. 1992), residual flux is often seen on unilluminated portions of the FOS detector's linear diode array at wavelengths shortward of 1600 Å, the red detector's faceplate cutoff. The residual flux is due to scattered light and/or errors in the background subtraction algorithm. In the 3CR 196 observations, an unilluminated region of the array 300 quarter-diode pixels wide and adjacent to the 3CR 196 spectrum was used to determine the background and any uniformly distributed scattered light. The scattered light/residual background was determined after all the subexposures from each orbit were added together. The predicted background is 0.011 counts s^{-1} $pixel^{-1}$. A residual flux of 2×10^{-4} counts s^{-1} $pixel^{-1}$ remains in the unilluminated region after dark subtraction, and this was assumed to be scattered light. After subtraction of this contribution, a flux of 1.8×10^{-3} counts s^{-1} $pixel^{-1}$ remains in the region between $\approx$1610 Å and the sharp rise in the spectrum near 1700 Å. Whether this is residual flux below the Lyman limit at $z_a = 0.871$ or a feature in the scattered light is unknown (see § 2.2.2); the data are analyzed with three different estimates of the scattering function. Any residual scattered light is of less importance at longer wavelengths because of the sharp rise in the sensitivity function.

2.2.2. *Spectral Modeling*

Although Lyα at $z_a = 0.437$ appears strong, we cannot assume that this feature is entirely due to that line because of wavelength coincidences with lines from higher levels of H I at $z_a = 0.871$. The rarely observed lines of S VI $\lambda\lambda$933.4, 944.5 may be important at $z_a = 0.871$ (see § 3.4 and Fig. 3*b*) and would also be blended with Lyα at $z_a = 0.437$.

Because of the low resolution and complexity of the spectrum, we can decompose the blend near Lyα at $z_a = 0.437$ only by modeling the spectrum. We fitted models to the data with the column densities of the strongest lines as free parameters. Different scattered light profiles and high ion b values were tried (see below) but were held fixed for each model.

There is no strong evidence in our spectrum for lines in the $z_a = 0.437$ system other Lyα, C IV, and Si II λ1526 (at $\lambda_{obs} = 2193.6$). The Si II line and the low-ionization lines measured by FCW are strong compared with lines in most high-redshift damped Lyα systems. For this reason, other neutral and singly ionized elements that are known to absorb strongly in low-ionization QSO absorption systems are included in the model

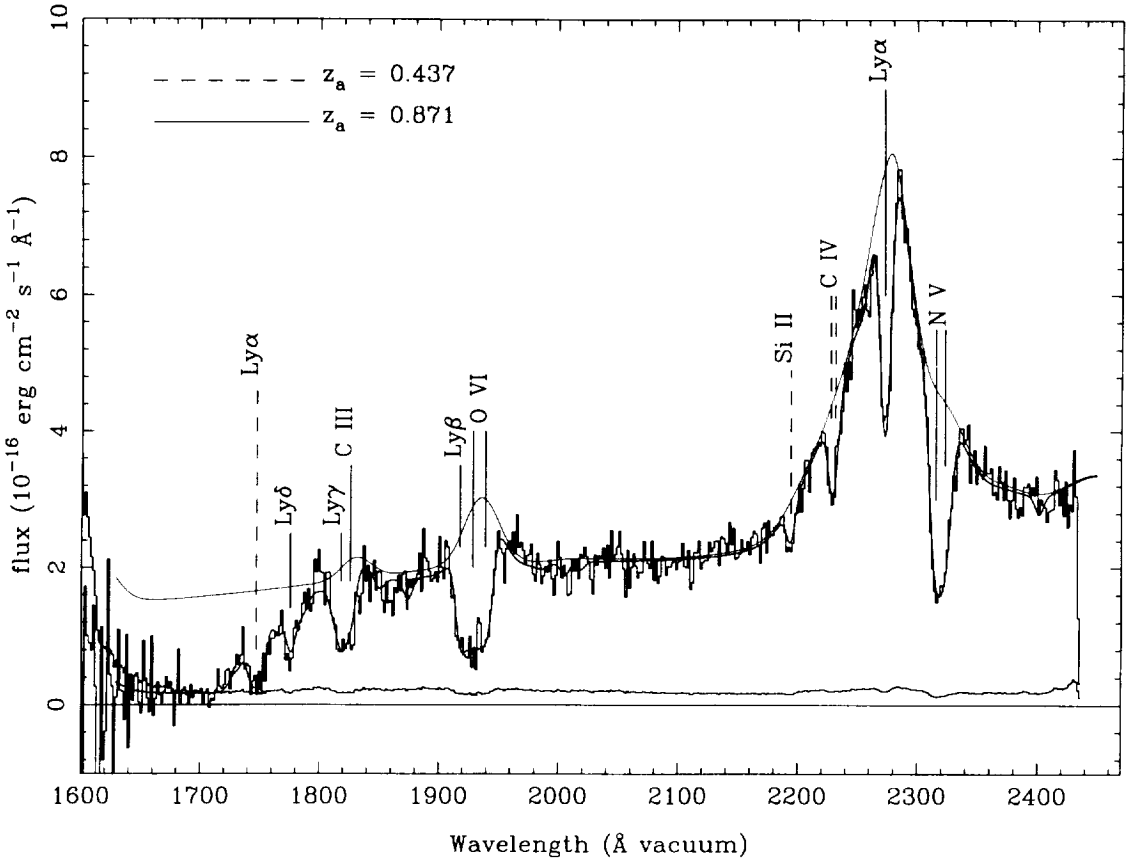

FIG. 3*a*

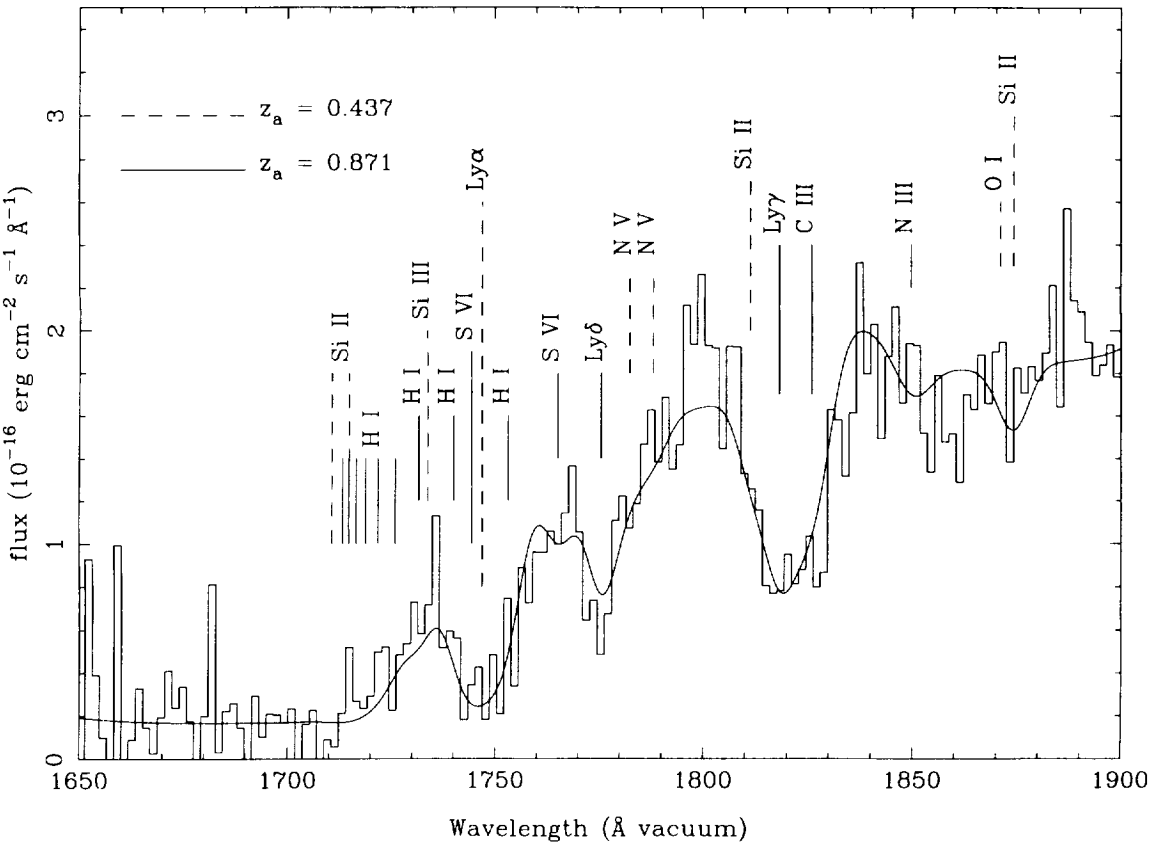

FIG. 3*b*

FIG. 3.—(*a*) Quasar spectrum with the best-fit (model 6, *heavy line*) and continuum (*thin line*) superposed. Features included in the model are marked. Solid lines indicate features in the $z_a = 0.871$ system; dashed lines indicate features in the $z_a = 0.437$ system. (*b*) Same as (*a*), expanded near Lyα at $z_a = 0.437$.

with fixed column densities chosen to reproduce the observed features or consistent with no detection. The strongest line of Si II usually is λ1260.4 (λ_{obs} = 1811.0), which does appear to be present in the blue wing of Lyγ in the z_a = 0.871 system. Similarly, some higher ionization lines whose presence is consistent with the detection of C IV are also included.

In the z_a = 0.871 system, we considered for inclusion in our models lines which were detected in the UV spectrum of the BAL QSO 0226−1024 (Korista et al. 1992). In addition to the strong lines mentioned in § 2.2, lines of Si III, S IV, and N III were included, at fixed values consistent with their nondetection in our spectrum. The lack of detection of any singly ionized lines in our spectrum is consistent with the strength of Mg II $\lambda\lambda$2796, 2803 observed in the optical (approximately 0.5 Å rest equivalent width) and the equivalent width limit of our spectrum.

Details of the fitting routines are as follows.

1. The shape of the continuum short of Lyβ/O VI in the z_a = 0.871 system is not known with high precision. We modeled it as a power law corrected for Galactic reddening [$E(B-V)$ = 0.05] and corrected in a statistical fashion for the unresolved Lyα forest absorption. For the statistical correction, we used a routine kindly provided by L. Zuo with parameters chosen to match the model 1 fit to the low-redshift Lyα forest from the *HST* QSO absorption-line key project (Bahcall et al. 1993).

2. Emission lines were fitted by multicomponent Gaussians. Lyα emission was modeled by two Gaussians; weaker lines have the same redshift and line width as the narrower Lyα component.

3. The wavelength zero point was set by assuming that the redshift of Si II λ1526 is z_a = 0.43685 (see § 2.2.1). The actual redshifts of both absorption systems were free parameters; the lower redshift falls in the range $0.43652 \leq z \leq 0.43765$ depending on the fit.

4. For any reasonable estimate of the instrumental profile, the high ions at z_a = 0.871 must have a high velocity dispersion. We used b = 350, 500, and 750 km s^{-1}. A good fit to the O VI absorption lines was impossible for $b < 350$ km s^{-1}.

5. The strong absorption lines are fitted with Voigt profiles. The column density of C III in the z_a = 0.871 system was fitted once for each of the velocity dispersions and then held fixed; the column densities of N V, O VI, and S VI were free parameters.

6. Although the presence of four Lyman lines in the z_a = 0.871 system should constrain the column density, velocity dispersion, and line-spread function, it is apparent that the observed Lyα absorption is too weak with respect to Lyβ. Any emission feature that cancels the absorption profile, either a feature intrinsic to the quasar emission-line region, or emission from an extended emission-line region, must be an extremely good match to the absorption wavelength because the cancellation between the emission and narrow absorption occurs before the smoothing introduced by the instrumental resolution. The strength of the Lyβ absorption which falls in the (usually) weak Lyβ/O VI emission line suggests instead that the z_a = 0.871 absorbing gas completely covers the continuum source but only partially covers the emission-line region, resulting in an apparently weak Lyα absorption line. In our models the covering factor of the lines at z_a = 0.871 was a free parameter. The assumption of partial emission-line covering does not have a large effect on the column densities of the high ions.

7. The entire model spectrum was convolved with an estimate of the FOS instrumental profile, which has a Gaussian core of 8.25 Å FWHM (5.0 channels) plus Lorentzian wings for scattered light. Rosa (1993) demonstrated that scattered light can be important for red objects observed with the FOS in the UV; it can also be important for any object with a sharp cutoff in the spectrum. We used three different values (including zero) for the width of the Lorentzian wings and fraction of light contained in them. In the models with broad wings, essentially all of the extension shortward of the Lyman limit at z_a = 0.871 is scattered light; in the models with Gaussian line-spread functions, this extension is largely real. The primary result of increasing the scattered light fraction is to increase the apparent optical depth below the Lyman limit. Although a greater H I column at z_a = 0.871 increases the strengths of the lines that are blended with the damped Lyα line, this effect is counterbalanced in part by the increase in the amount that the damped line is filled in by scattered light and the increase in the "blackness" of the line core. Thus, the effect of changes in the scattered light on the computed value of N(H I) at z_a = 0.437 cannot easily be predicted.

In Table 1, we present the most important fixed parameters for nine models and the derived H I column density at z_a = 0.437. The column labeled "LSF Wings" indicates which of the three scattered light profiles was assumed (see above). In Table 2, we present the results for the z_a = 0.871 gas. Here, "covering factor" indicates the best fit to the fraction of the broad emission line region covered by the gas at z_a = 0.871 (see above and § 3.4). These models have 21 free parameters and χ^2 per degree of freedom of approximately 1.3, indicating that our model is an incomplete description of the data. Because all values of χ^2 for these models are similar, we chose as our best fit model 6, which gives subjectively the best agreement for the greatest number of features. That model is shown in Figures 3*a* and 3*b*.

3. ANALYSIS

3.1. *Southeast Galaxy*

The object southeast of the QSO (object G1 of BB) is now revealed as a fairly normal barred spiral galaxy centered 1".56 ± 0".05 from the quasar. It shows a prominent bar broken into knots; extending from the ends of the bar are two spiral arms, more than 8".5 across from end to end. Fainter than the bar, a central bulge or disk is seen. The appearance of the galaxy leads to a classification of SBc. The presence of the arms and the relatively low spatial resolution make the measurement of orientation and inclination somewhat subjective, but the major axis, as defined by the outer isophotes of the disk, is oriented

TABLE 1

MODEL PARAMETERS AND H I COLUMN DENSITY FOR THE z_a = 0.437 SYSTEM

Model	b High Ions (km s^{-1})	LSF Wings	N(H I) (10^{20} cm^{-2})
1	350	None	0.49
2	350	Medium	0.96
3	350	Broad	1.11
4	500	None	0.58
5	500	Medium	1.18
6	500	Broad	1.47
7	750	None	0.27
8	750	Medium	0.44
9	750	Broad	1.45

TABLE 2

RESULTS FOR THE $z_a = 0.871$ SYSTEM

MODEL	COVERING FACTOR	b H I (km s^{-1})	log [N(cm^{-2})]				
			H^0	C^{+2}	N^{+4}	S^{+5}	O^{+5}
1.....	0.38	240	17.5	15.2	15.8	15.3	17.8
2.....	0.56	220	17.6	15.2	16.7	15.3	17.5
3.....	0.50	210	17.8	15.2	16.5	15.3	17.5
4.....	0.39	220	17.6	14.9	15.7	15.3	16.3
5.....	0.61	210	17.7	14.9	16.0	15.2	17.1
6.....	0.54	210	17.8	14.9	16.0	15.2	17.2
7.....	0.46	200	17.6	14.9	15.7	15.3	16.2
8.....	0.67	190	17.7	14.9	15.8	15.3	16.2
9.....	0.64	180	17.8	14.9	15.8	15.3	16.3

approximately 28° to a line between the galaxy center and the QSO, and the galaxy is inclined 63° to the line of sight. The integrated count rate for the southeast galaxy is 8.39 counts s^{-1}, corresponding to 1.49×10^{-17} ergs cm^{-2} s^{-1} Å^{-1} ($m_{6942} = 20.4$ or $R \approx 20.2$). Approximately 75% of the flux is contained in the central disk and bar. The flux determination is statistically quite accurate, but systematic errors due to PSF subtraction are difficult to quantify. They are probably less than 0.1 mag within the region measured.

As yet, we have no proof that the galaxy is at the 21 cm redshift. It could be at either of the previously known absorption redshifts, or it could be at a completely unrelated redshift. Without a redshift measurement, we can judge the likelihood that the galaxy is at a random redshift by the probability of finding a galaxy of at least this brightness near the quasar. Shanks et al. (1984) find approximately 3600 galaxies per square degree brighter than $R = 20.2$. Thus, the probability that a galaxy as bright as the southeast galaxy would be found within 3.″0 of the quasar by chance is only 0.008. While we cannot draw any real statistical inferences from such an a posteriori calculation for a single object, it seems plausible that, with such a low probability of chance occurrence, this galaxy is associated with one of the two redshifts already associated with this quasar.

Assuming that the spiral galaxy is at $z = 0.437$, and making no correction for reddening, either in the object or the Galaxy, we derive $M_B = -21.3$. This is $1.3L_*$. At $z = 0.871$, on the other hand, we derive $L = 11.7L_*$. Thus, we suggest, as do BB, that the southeast galaxy is the object responsible for the $z_a = 0.437$ absorption.

Bosma (1981) has shown that the H I column density in spiral galaxies exceeds 2×10^{20} cm^{-2} within 1.5 Holmberg radii. However, the outer regions of this galaxy, as defined at an isophote 1 σ above the background noise, have a surface brightness $B_{\rm surf} = 24.0$ mag per square arcsecond, corrected for redshift, much brighter than $B_{\rm surf} = 26.5$ mag per square arcsecond, the isophotal magnitude at which the Holmberg radius is measured. Thus, we must estimate the H I extent ($R_{\rm lim}$) from a scaling law. Following Wolfe et al. (1986) and assuming no luminosity evolution,

$$R_{\rm lim} = 34.5\left(\frac{L}{L_*}\right)^{0.4} h^{-1}\ {\rm kpc} = 38.3\ h^{-1}\ {\rm kpc}\ .$$

At $z = 0.437$, the projected separation of the quasar and galaxy center is 11.5 h^{-1} kpc, and the quasar sight line intersects the inclined disk of the galaxy approximately 16 h^{-1} kpc from its center, well within $R_{\rm lim}$. Thus, a strong Lyα line should be seen in the quasar spectrum.

3.2. *Northern and Southern Amorphous Objects*

An amorphous object, also discussed by BB (their object G2), lies 1.″28 ± 0.″05 north of the quasar. The integrated flux of this object is 2.1×10^{-18} ergs cm^{-2} s^{-1} Å^{-1}, corresponding to $m_{6942} = 22.6$ or $R \approx 22.3$. Extending from the region of unreliable PSF subtraction to approximately 1.″2 south of the quasar is a poorly defined extension, approximately as bright as the northern object, but too close to the quasar to measure reliably. This is probably not a feature of the PSF, as it appears both in our best fit and in images where the PSF is clearly oversubtracted. This extension was not seen by BB, possibly because it is too close to the quasar position.

BB suggested that the northern object is a galaxy at $z = 0.871$. If the northern object is at $z = 0.871$, we derive $M_B = -21.6$ or $L = 1.7L_*$. At this redshift, the impact parameter is 12.9 h^{-1} kpc, and a normal galaxy might be expected to show a damped Lyα absorption in the spectrum of the quasar. The lack of such an absorption at $z_e = 0.871$ may be an indication that the northern object is not a galaxy or that it is a galaxy affected by its proximity to the quasar (see § 3.4). BB suggested that the proximity of this object to the northeast radio hot spot might indicate that it lies along the radio jet, and that gas blown out of this galaxy by the interaction with the radio jet is responsible for the $z_a = 0.871$ absorption. The approximate alignment of both hot spots, the northern object, and the southern extension suggest some relation between the optical objects and the radio jets. Fabian et al. (1988) detected extended emission in the field of 3CR 196, through a spectrograph slit which probably included part of the northern object. Since the filter bandpass used for our WFC observations includes [O II] λ3727 at $z_e = 0.871$, it is possible that the northern and southern amorphous objects actually consist of extended emission-line gas, similar to that seen aligned with the radio jets in many high-redshift radio galaxies.

If instead the northern object is at $z = 0.437$, then we derive $M_B = -19.2$, or $L = 0.18L_*$. The impact parameter is 9.5 h^{-1} kpc. If the object is a spiral galaxy, and if the scaling law given above for $R_{\rm lim}$ is applicable, this object would cause damped Lyα absorption at the quasar position. The 21 cm absorption in front of the northeast hot spot would be consistent with the limit of Brown et al. (1988), but it is unlikely that the gas would extend across the other portions of the radio lobes. Steidel, Dickinson, & Persson (1994a) find that galaxies as faint as $M_B = -19.0$ can produce Mg II absorption. Two galaxies this faint are, in fact, suspected to give rise to low-redshift damped Lyα (Steidel et al. 1994b, 1995; Cohen et al. 1995). Without observations to determine the redshift of the northern object, we cannot rule out a contribution from this object to the

damped Lyα or metal-line absorption at $z_a = 0.437$. Perhaps the low ionization metal lines at $z_a = 0.437$ are as broad as they are (FCW) because they contain contributions from two galaxies.

3.3. *Spectrum of the $z_a = 0.437$ Absorber*

The details of the spectral models are presented earlier in § 2.2.2. The model chosen as the best fit to the $z_a = 0.437$ system without regard to the H I column density had an H I column density of 1.47×10^{20} cm^{-2}. Since all the values found range between 2.7×10^{19} cm^{-2} and 1.5×10^{20} cm^{-2} (Table 1), it is clear that some Lyα must be present; the S VI lines from the $z_a \approx z_e$ system cannot be used to fit the entire blend. If, however, we omit the S VI lines, a region of the spectrum in the Lyα red wing remains below the model, regardless of the H I column density. Although this excess absorption could be due to the presence of a Lyα forest line, the strength of the N V lines and the relative ionization and abundance of N V and S VI require that under most circumstances the S VI lines must be substantial (see § 3.4). We conclude that a high H I column exists along the line of sight to the optical quasar, at least 11.5 h^{-1} kpc from the southeast galaxy center (assuming a face-on galaxy), and 15–20 h^{-1} kpc from the site of the 21 cm absorption.

The H I column density over a significant fraction of the radio lobes must be higher than measured in front of the optical quasar in order to produce the 21 cm absorption. This might be expected because the optical quasar is farther from the center of the galaxy than the closest extensions of the radio emission. At the eastern hot spot, $\tau_{21\,\mathrm{cm}} \leq 0.08$ (Brown et al. 1988); this limit is not very restrictive but is consistent with the location of this hot spot, which is farther from the galaxy center than the optical quasar or the other portions of the radio lobes.

If the southeast spiral galaxy has a gaseous disk that extends beyond the visible arms with a column density of a few times 10^{20} cm^{-2}, as is typical for spiral galaxies, then it could easily cover both radio lobes. If $T_s = 300$ K, as is typical of the Galaxy, then with $b = 10$ km s^{-1}, the optical depth would be consistent with the limit of Brown et al. (1988) that $\tau_{21\,\mathrm{cm}} \geq 0.026$ over a portion of the extended radio structure. Because the radio and optical absorption regions are clearly not coincident, we cannot comment on the spin temperature.

A perplexing question is why there are not two 21 cm absorption components separated by a few hundred kilometers per second, since the projected velocity difference of the two spiral arms should be quite large. Although the eastern lobe is considerably closer to the galaxy than the western lobe and hot spot, it is possible that the absorption comes from the western hot spot. Interpolation of the 408 and 1666 MHz fluxes given by Lonsdale (1984) to the redshifted 21 cm frequency suggests that the flux in the diffuse component of the eastern lobe may be too low to have permitted a detection of weak 21 cm absorption in the initial observation of Brown & Mitchell (1983). (However, Lonsdale suggests that the 1666 MHz flux of that component may be underestimated.) Any sharp second radio component may fall outside the window observed at a higher signal-to-noise ratio by Brown & Mitchell (1983), or the absorption might be smeared out by the velocity gradient across the diffuse radio lobes. The small velocity difference (≈ 50 km s^{-1}) between the radio and optical absorption systems also needs to be explained.

For a high column density absorber, it might be possible to infer the dust-to-gas ratio (which has implications for both the metallicity and UV background) from the continuum shape. However, a Galactic dust-to-gas ratio and $N(\mathrm{H\ I}) = 1.5 \times 10^{20}$ cm^{-2} imply $E(B-V) = 0.03$,[6] which would have negligible effect on the continuum for which the intrinsic shape is, in any case, unknown at that level. BB point out that the color of 3CR 196 is consistent with $E(B-V) = 0.15$ at $z = 0.437$; this color index is not consistent with our measurement of N(H I).

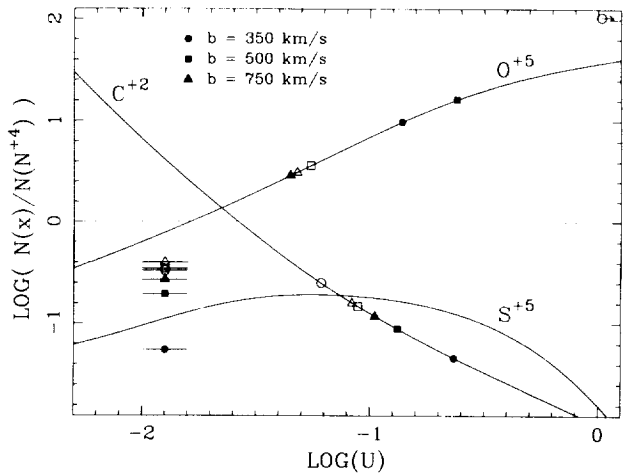

FIG. 4.—Abundance of C^{+2}, S^{+5}, and O^{+5} with respect to N^{+4} as a function of ionization parameter. Relative abundances for C^{+2} and O^{+5} from our model fits to the spectra are indicated on the curves at the appropriate ionization parameter. The symbols indicating the S^{+5} abundance are marked near the left of the figure because the ionization parameter is not tightly constrained. Solid symbols indicate the three models with broad wings on the line-spread function; open symbols indicate the three models with Gaussian line-spread functions.

3.4. *Spectrum of the $z_a \approx z_e$ Absorber*

Column densities for the ions in the $z_a = 0.871$ system are given in Table 2. Abundances relative to hydrogen are not meaningful, because the best-fit velocity dispersion of the Lyman lines ($b \approx 200$ km s^{-1}) is clearly different from that of the higher ionization lines. Figure 4 presents the relative abundances of the metal ions as a function of ionization parameter, $U = N_\gamma/4\pi n_e r^2 c$. These were calculated with CLOUDY (version 80.06, Ferland 1991), using the standard active galactic nucleus (AGN) continuum, solar abundances, $n_e = 10^8$ cm^{-3}, and $N_c = 10^{18}$ cm^{-2}. While a single ionization parameter, $U \approx 0.1$, is consistent with all metal-line strengths for models with broad wings in the line-spread function, we can realistically only limit the ionization parameter to $0.03 \lesssim U \lesssim 0.3$ for single-zone models. The high ionization and broad line widths (which imply turbulence or multiple components) suggest that the $z_a = 0.871$ gas is related to the BAL QSO phenomenon.

Note that the calculated abundance of S^{+5} relative to N^{+4} varies by less than a factor of 2 over a wide range of ionization parameter. This suggests that it would be inappropriate to model this spectrum with a considerably larger or smaller contribution from S VI than was determined here. Higher resolution observations to refine the S^{+5}/N^{+4} ratio could determine the relative abundance of these elements without requiring an accurate measurement of U.

Assuming that the high-ionization absorption occurs in clouds ionized by the quasar, we can derive the distance of the

[6] We assume $N(\mathrm{H\ I}) = 4.93 \times 10^{21} E(B-V)$ (Diplas & Savage 1994).

cloud(s) from the quasar,

$$d = 14.6 \sqrt{\frac{10^6}{n_e U}}\, h^{-1} \text{ pc} .$$

If $n_e \geq 10^6$ cm^{-3}, as has been suggested for BAL QSOs (Turnshek 1984), then the $z_a \approx z_e$ absorber is no more than 46 h^{-1} pc from the central source. At that distance, it may be outside the broad-line region (BLR), which has a 1–10 pc radius in the conventional picture. If we assume that all the nitrogen is N^{+4}, that abundances are solar ($\log N/H = -3.95$), and that n_e equals $n(H)$, then for model 6, the total path length through the absorbing clouds(s), t_c, is $26.4 n_e^{-1}$ pc. If the absorber is nearby, just outside the BLR, the density must be large, as derived above. Thus, any nearby absorber must be made up of many small clouds (if their diameter is similar to their depth), which might not completely cover the BLR. (Alternatively, there might be an extended BLR located outside the $z_a \approx z_e$ absorber and the conventional BLR, which is not covered by the absorbing clouds.) If the north object is a galaxy whose line of sight distance from the quasar is similar to the lateral separation, clouds in the ISM could be ionized by the quasar continuum. At the assumed ionization parameter and that distance, the clouds which make up the absorber would have $n_e \approx 13$ cm^{-3}, and the cloud thickness would be $t_c \approx 2$ pc. Such clouds might also reasonably be expected to only partially cover the quasar BLR.

The properties of the $z_a \approx z_e$ absorber can be summarized as follows:

1. The region producing the absorption at the emission redshift consists of at least two zones of different velocity dispersion. At least one of these zones is highly ionized.
2. The ionization parameter of the highly ionized region is similar to that required for BALQSOs (Barlow 1993), and thus it is possible that density and distance from the central source are similar as well.
3. The absorbing clouds may cover only 50% of the BLR along the line of sight. If the absorbing region is close to the central source, then the absorbing clouds are very small.

4. DISCUSSION

Our results on the 21 cm absorber can be summarized as follows:

1. An apparently normal spiral galaxy with luminosity $1.3L_*$, if at $z = 0.437$, has spiral arms which clearly cross a portion of the both radio lobes. Such a galaxy should give rise to 21 cm absorption.
2. The H I column density [N(H I) $\approx 1.5 \times 10^{20}$ cm^{-2}] at the position of the QSO, less than 1 Holmberg radius from the galaxy center and at least 15 h^{-1} kpc from the site of the 21 cm absorption, is almost high enough to be included in samples of "damped Lyα systems" in QSO spectra.

Conceivably, the radio and/or optical absorptions are due to unseen dwarf galaxies, and the barred spiral galaxy we detect close to the line of sight is just a chance interloper. Alternatively, the galaxy could be at $z = 0.437$, but the absorption could be due to unusual absorption regions such as tidal tails. However, the presence of high column density absorption in at least two widely separated locations, each within 1.5 Holmberg radii of a galaxy whose luminosity is such that it should possess a large gaseous disk, makes it highly probable that the various H I observations of this system are best explained by an extended, high column density gaseous disk associated with a normal, luminous spiral galaxy.

Three other low redshift systems, PKS 1229−021 (Steidel et al. 1994b; Cohen et al. 1995), 3CR 286 (Meyer & York 1992; Cohen et al. 1994; Steidel et al. 1994b), and PKS 0454+039 (Steidel et al. 1995), have measurements of the H I column in a damped system and tentative identifications of the absorbers. In none of these cases (or in 3CR 196) has the redshift of the candidate been measured. Four cases are not enough from which to draw firm conclusions on the origin of 21 cm and damped Lyα systems, but the range of properties is interesting. While the candidate absorber in 3CR 196 is a luminous spiral galaxy, the PKS 1229−021 ($z_a = 0.395$) and PKS 0454+039 ($z_a = 0.860$) candidate absorbers are near the lower limit of luminosity for the class of Mg II absorbers. The 3CR 286 ($z_a = 0.692$) candidate absorber is a luminous but low surface brightness galaxy. In both the PKS 1229−021 and PKS 0454+039 absorbers, T_s appears to be normal, while it may be as high in the 3CR 286 absorber as in the high-redshift systems. Metal abundances in the 3CR 286 and PKS 0454+039 absorbers are low.

Whether the differences are related to the differences in fundamental properties of these galaxies or to their particular evolutionary stages is unknown. Even a comparison of the metal abundances to solar is obscured by uncertainties in the ages of the absorption-line systems caused by the large uncertainty in H_0. Metal abundance measurements in the 3CR 196 and PKS 1229−021 absorption systems would make an interesting comparison because the 3CR 196 absorber is a luminous galaxy of normal appearance, while the PKS 1229−021 absorber has a low luminosity, similar to the PKS 0454+039 absorber. Unfortunately, the weak lines of Zn II and Cr II fall in the UV for those systems and are probably unobservable, so abundance determinations will have to rely on other lines. Accurate abundance measurements may not be possible even with very high resolution, high signal-to-noise ratio spectroscopy, however, because of blending of the multiple components of strong lines. For 3CR 196, a higher resolution FOS spectrum is needed to determine the H I column density more precisely; this observation would take seven *HST* orbits.

Low surface brightness objects are now being found in large numbers at low redshift (see, e.g., Schombert et al. 1992). McGaugh & Bothun (1994) argue that these are galaxies which began star formation late and have evolved slowly. They could account for the excess of faint blue galaxies (McGaugh 1994). Identification of a damped Lyα system within this population would clearly be important for our understanding of such systems. Steidel et al. (1994b) suggest that the low metal abundances observed in the 3CR 286 system are a natural consequence of the low star formation rate in such a low surface brightness galaxy. Alternatively, the candidate 3CR 286 absorber could be a low surface brightness extension of a more normal galaxy centered on the QSO.

Redshift determinations for the candidate absorbers will be difficult but are necessary for our understanding of these systems. Imaging of more such systems, found either from radio surveys or *HST* surveys for low-redshift damped Lyα lines, is required to determine the fraction that is due to normal spirals. A galaxy identified in the field of 4C 39.47 (Hintzen et al. 1989) is potentially very similar to the galaxy along the line of sight to 3CR 196. The galaxy at $z = 0.366$ lines 28 h^{-1} kpc from the line of sight to the quasar. Mg II absorption with an equivalent width of approximately 1 Å (rest) has been detected

at that redshift (Womble 1992). With type Sbc (from the luminosity profile) and $L = 1.7L_*$, this object should produce a damped Lyα line. An *HST* study of this galaxy would help to characterize the H I column density and metal abundance as a function of galaxy type and impact parameter at moderate redshifts.

We thank E. M. Burbidge, F. Hamann, A. Oren, H. E. Smith, A. Wolfe, and D. Womble for helpful discussions. W. Keel provided a digitized version of Kennicutt's galaxy spectra. J. Krist provided his CCD pixel response functions in advance of publication and advised us on the proper use of Tiny Tim. M. Loveland prepared the PSFs using Tiny Tim. A. Oren provided the radio map of 3CR 196. An anonymous referee offered helpful suggestions for improving this paper. This work is part of GHRS GTO observations and is supported by NASA grant NAG 5-1858.

REFERENCES

Bahcall, J. N., et al. 1993, ApJS, 87, 1
Barlow, T. A. 1993, Time Variability of Broad Absorption Line QSOs, Ph.D. thesis, Univ. of California, San Diego
Bartko, F., Burks, G., Kriss, G., Davidsen, A., Cohen, R., Junkkarinen, V., Lyons, R., & Harms, R. 1993, in Space Astronomical Telescopes and Instruments II, Vol. 1945, ed. P. Y. Bely & J. B. Breckinridge (Orlando: SPIE), 318
Black, J. H., Chaffee, F., & Foltz, C. 1987, ApJ, 317, 442
Boissé, P., & Boulade, O. 1990, A&A, 236, 291 (BB)
Bosma, A. 1981, AJ, 86, 1825
Briggs, F. H. 1987, in QSO Absorption Lines: Probing the Universe, ed. J. Blades, D. Turnshek, & C. Norman (Baltimore: STSCI), 275
Briggs, F. H., Wolfe, A., Liszt, H., Davis, M. & Turner, K. 1989, ApJ, 341, 650
Brown, R. L., Broderick, J. J., Johnston, K. J., Benson, J. M., Mitchell, K. J., & Waltman, W. B. 1988, ApJ, 329, 138
Brown, R. L., & Mitchell, K. J. 1983, ApJ, 264, 87
Caganoff, S., Tsvetanov, Z., & Armus, L. 1992, Instrument Sci. Rep. CAL/FOS-081
Chaffee, F., Black, J., & Foltz, C. 1988, ApJ, 335, 584
Cohen, R. D., Barlow, T. A., Beaver, E. A., Junkkarinen, V. T., Lyons, R. W., & Smith, H. E. 1994, ApJ, 421, 453
Cohen, R. D., Beaver, E. A., Junkkarinen, V. T., Lyons, R. W., & Diplas, A. 1995, in preparation
Diplas, A., & Savage, B. D. 1994, ApJ, 427, 274
Fabian, A. C., Crawford, C. S., Johnstone, R. M., Allington-Smith, J. R., & Hewett, P. C. 1988, MNRAS, 235, 13P
Fall, S. M., Pei, Y., & McMahon, R. 1989, ApJ, 341, L5
Ferland, G. J. 1991, Hazy, OSU Astron. Dept. Internal Rep. 91-01
Foltz, C., Chaffee, F., & Black, J. 1988, ApJ, 324, 267
Foltz, C. B., Chaffee, F. H., Jr., & Wolfe, A. M. 1988, ApJ, 335, 35 (FCW)
Hayes, D. S., & Latham, D. W. 1975, ApJ, 197, 593
Hintzen, P., Romanishin, W., Foltz, C., & Keel, W. 1989, ApJ, 337, L5
Junkkarinen, V. T., Beaver, E. A., Cohen, R. D., Hier, R., Lyons, R., & Rosenblatt, E. 1992, Instrument Sci. Rep. CAL/FOS-066
Kennicutt, R. C. 1992, ApJS, 79, 255
Koornneef, J., Bohlin, R., Buser, R., Horne, K., & Turnshek, D. 1988, in Highlights of Astronomy, Vol. 7, ed. J.-P. Swings (Dordrecht: Reidel), 833
Korista, K. T., et al. 1992, ApJ, 401, 529
Krist, J. 1993, in ASP Conf. Proc. 52, Astronomical Data Analysis Software and Systems II, ed. R. J. Hanisch, R. J. V. Brissenden, & J. Barnes (San Francisco: ASP), 530
Lanzetta, K. M., Wolfe, A., & Turnshek, D. A. 1989, ApJ, 344, 277
Lanzetta, K. M., Wolfe, A., Turnshek, D., Lu, L., McMahon, R., & Hazard, C. 1991, ApJS, 77, 1
Lonsdale, C. J. 1984, MNRAS, 208, 545
Lyons, R. W., Baity, W., Beaver, E. A., Cohen, R. D., Junkkarinen, V. T., Linsky, J. B., & Rosenblatt, E. I. 1992, Instrument Sci. Rep. CAL/FOS-080
Lyons, R. W., Beaver, E. A., Cohen, R. D., & Junkkarinen, V. T. 1994, Instrument Sci. Rep. CAL/FOS-111
Matthews, T. A., & Sandage, A. R. 1963, ApJ, 138, 30
McGaugh, S. S. 1994, Nature, 367, 538
McGaugh, S. S., & Bothun, G. D. 1994, AJ, 107, 530
Meyer, D. M., & York, D. G. 1992, ApJ, 399, L121
Oke, J. B., & Gunn, J. E. 1983, ApJ, 266, 713
Pei, Y., Fall, S. M., & Bechtold, J. 1991, ApJ, 378, 6
Pettini, M., Smith, L. J., Hunstead, R. W., & King, D. L. 1994, ApJ, 426, 79
Rosa, M. R. 1993, in Calibrating *Hubble Space Telescope*, ed. J. C. Blades & S. J. Osmer (Baltimore: STScI), 190
Schombert, J. M., Bothun, G. D., Schneider, S. E., & McGaugh, S. S. 1992, AJ, 103, 1107
Shanks, T., Stevenson, P. R. F., Fong, R., & MacGillivary, H. T. 1984, MNRAS, 206, 767
Steidel, C. C., Bowen, D. V., Blades, J. C., & Dickinson, M. 1995, ApJ, 440, L45
Steidel, C. C., Dickinson, M., & Persson, S. E. 1994a, ApJ, 437, L75
Steidel, C. C., Pettini, M., Dickinson, M., & Persson, S. E. 1994b, AJ, 108, 2046
Trauger, J. T., et al. 1994, ApJ, 435, L3
Turnshek, D. A. 1984, ApJ, 278, L87
Turnshek, D. A., Wolfe, A. M., Lanzetta, K. M., Briggs, F. H., Cohen, R. D., Foltz, C. B., Smith, H. E., & Wilkes, B. J. 1989, ApJ, 344, 567
Wolfe, A. M., Briggs, F., Turnshek, D., Davis, M., Smith, H. E., & Cohen, R. D. 1985, ApJ, 294, L67
Wolfe, A. M., Turnshek, D. A., Smith, H. E., & Cohen, R. D. 1986, ApJS, 61, 249
Womble, D. S. 1992, The Extent and Content of Low Ionization Gas in Galaxies, Ph.D. thesis, Univ. of California, San Diego
York, D. G., Dopita, M., Green, R., & Bechtold, J. 1986, ApJ, 311, 610

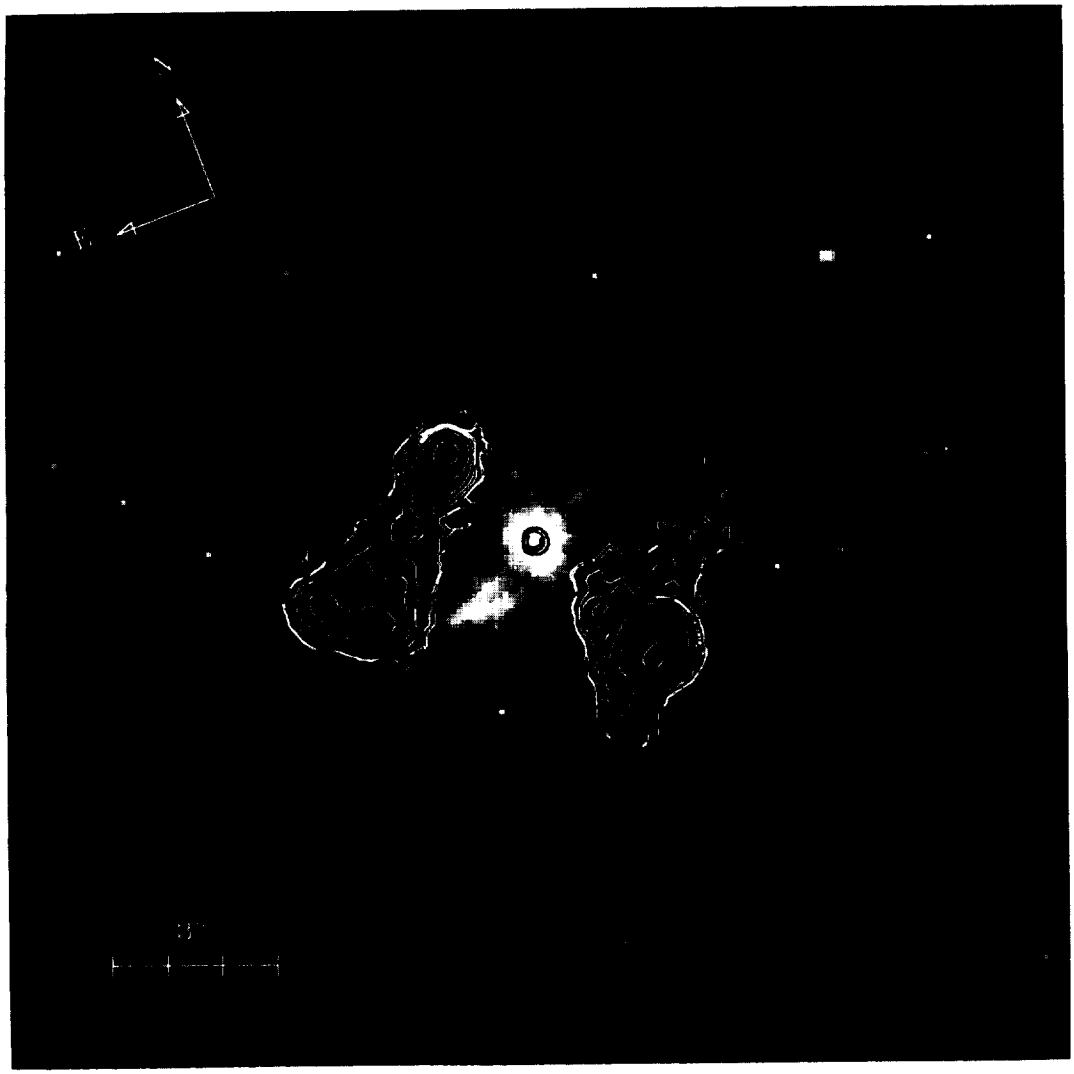

FIG. 1.—Portion of the averaged WFC image centered on 3CR 196. The scaling of the data is logarithmic. The arrows indicate north and east. The scale is indicated by a 3".0 long line. The 6 cm flux contours provided by A. Oren are superposed.

PLATE 2

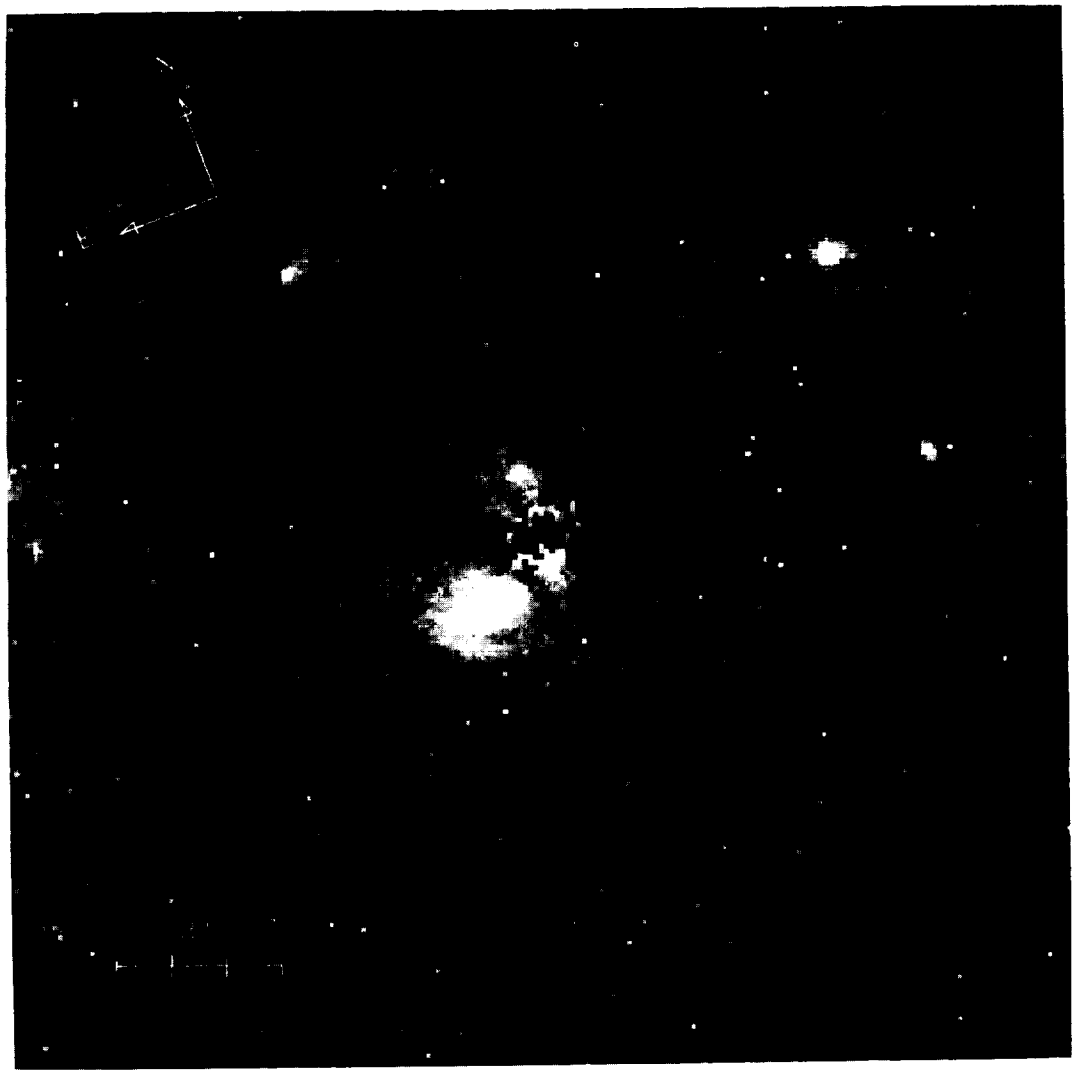

FIG. 2.—Averaged WFC image after subtraction of the computed PSF. The scaling of the data is logarithmic in order to show the inner regions of the southeast galaxy as well as the faint outer regions. The arrows and scale are as in Fig.1